Spectral Image Fusion from Compressive Measurements Using Spectral Unmixing

Edwin Vargas
Department of Electrical Engineering
Universidad Industrial de Santander
Bucaramanga, Colombia 680002
Email: edwin.vargas4@correo.uis.edu.co

Henry Arguello
Department of Computer Science
Universidad Industrial de Santander
Bucaramanga, Colombia 680002
Email: henarfu@uis.edu.co

Jean-Yves Tourneret
University of Toulouse
INP-ENSEEIHT/IRIT/TéSA
Toulouse, France
Email: Jean-Yves.Tourneret.enseeiht.fr

***Abstract*—This work aims at reconstructing a high-spatial high-spectral image from the complementary information provided by sensors that allow us to acquire compressive measurements of different spectral ranges and different spatial resolutions, such as hyperspectral (HS) and multi-spectral (MS) compressed images. To solve this inverse problem, we investigate a new optimization algorithm based on the linear spectral unmixing model and using a block coordinate descent strategy. The non-negative and sum to one constraints resulting from the intrinsic physical properties of abundance and a total variation penalization are used to regularize this ill-posed inverse problem. Simulations results conducted on realistic compressive hyperspectral and multispectral images show that the proposed algorithm can provide fusion and unmixing results that are very close to those obtained when using uncompressed images, with the advantage of using a significant reduced number of measurements.**

I. Introduction

Hyperspectral (HS) sensors collect data that can be represented by a three-dimensional data cube [1]. This data cube referred to as HS image is a collection of 2D images, where each 2D image is captured at a specific wavelength. HS images are characterized by a high-spectral-resolution which allows an accurate identification of the different materials contained in the scene of interest. Analyzing the spectral information of HS images has allowed the development of many applications in the fields of remote sensing [2], medical imaging [3] or astronomy [4]. However, due to technological reasons, HS images are limited by their relatively low spatial resolution [5]. For instance, the Hyperion imaging spectrometer has about 220 spectral bands, which extend from the visible region (0.4 to 0.7 μm) through the SWIR (about 2.5 μm), with a spatial resolution of 30 m [6].

In addition to their reduced spatial resolution, conventional spectral imaging devices have the drawback of requiring to scan a number of zones that grows linearly in proportion to the desired spatial or spectral resolution. Finally, HS images require to acquire a large amount of data that must be stored and transmitted. To overcome this limitation, motivated by the compressed sensing (CS) theory [7], several spectral imagers have been recently proposed [8], [9], [10]. Compressive spectral imaging (CSI) techniques [11], [12] exploit the fact that HS images are sparse in some basis and can thus be efficiently compressed by using CS. As a consequence, the images acquired with CSI have a reduced number of measurements when compared to conventional spectral imaging devices, which makes them attractive for many practical applications.

To overcome the spatial resolution limitation, a common trend is to fuse images with different spectral and spatial resolutions. A typical example is the fusion of HS images (having high spectral resolution) with multispectral (MS) images (having high spatial resolution), which is studied in this work. Another example is HS pansharpening, which addresses the fusion of panchromatic and HS images [13]. Many algorithms have been proposed in the literature for image fusion (see [13] and [14] for recent reviews). To name a few, fast fusion algorithms based on spectral mixture analysis have been developed to fuse HS and MS images [15], [16]. The coupled nonnegative matrix factorization (CNMF) was also proposed to alternately estimate the endmember and abundance matrices [17].

Contrary to the previous fusion methods using conventional spectral images, this paper investigates a new algorithm allowing the fusion of compressed spectral images (HS and MS). Specifically, we propose a fusion algorithm to reconstruct a high-spatial high-spectral image represented as an $m_\lambda \times n$ matrix $\mathbf{X}$ from compressive measurements denoted as $\mathbf{Y}_h$ and $\mathbf{Y}_m$, resulting from HS and MS images. Note that m_λ is the number of spectral bands and that $n = n_r \times n_c$ is the number of pixels in each band. The proposed algorithm is based on the linear mixture model, which assumes that each pixel of the target image is a linear mixture of spectral signatures (referred to as endmembers). Thus, we can represent the target spectral image as $\mathbf{X} = \mathbf{MA}$, where $\mathbf{M} \in \mathbb{R}^{m_\lambda \times p}$ is the endmember matrix whose columns are spectral signatures, p is the number of materials contained in the image and $\mathbf{A} \in \mathbb{R}^{p \times n}$ represent the abundance fractions of the endmembers (see [18] for details).

In this work, we consider CSI devices such as those proposed in [8], [10], [19], where the measurements can be modeled as k linear projections of the spectral images using optical filters [20]. More precisely, given an arbitrary spectral image represented as the matrix $\mathbf{X} \in \mathbb{R}^{m_\lambda \times n}$, the spectral compressive measurements are calculated as $\mathbf{Y}_{i,j} = \sum_{l=0}^{m_\lambda - 1} \mathbf{H}_{i,l}\mathbf{X}_{l,j} + \omega_{i,j}$, where $\mathbf{Y} \in \mathbb{R}^{k \times n}$ are the compressive measurements with $k \ll m_\lambda$. Note that the ith row of $\mathbf{H} \in \mathbb{R}^{k \times m_\lambda}$ represents the spectral response of an optical filter sensing the spectral image to generate the ith projection. Note also that these optical filters can be selected randomly or designed as in [20], [21], [22], [23]. The additive term $\omega_{i,j}$ classically summarizes the errors between the proposed model and the observations. In matrix form, the compressive measurements can be rewritten as $\mathbf{Y} = \mathbf{HX} + \mathbf{N}$, where $\mathbf{N} \in \mathbb{R}^{k \times n}$ is the noise matrix. This discrete model will be used to describe the compressive measurements for the HS and MS images, i.e., for $\mathbf{Y}_h$ and $\mathbf{Y}_m$. Finally, it is important to mention that standard endmember extraction algorithms, such as VCA [24], SVMAX [25] or N-FINDR [26], cannot be used directly when the observed images have been compressed.

978-1-5386-1251-4/17/$31.00 ©2017 IEEE

The paper is organized as follows. Section II introduces the observation models used for the HS and MS images. The inverse problem considered for the proposed image restoration method is also formulated. The optimization algorithm investigated to solve this inverse problem is presented in Section III. Numerical results conducted on realistic HS and MS images are presented in Section IV whereas conclusions are reported in Section V.

II. Problem statement

This section formulates the data fusion problem considered in this paper to estimate a high spatial / high spectral resolution image from two compressed images with different spectral and spatial resolutions.

A. Observation models

It is very common to assume that HS and MS images result from the application of linear spatial and linear spectral degradations to a higher resolution image $\mathbf{X} = \mathbf{MA}$ [16] [27]. Moreover, as we mentioned before, we propose to consider compressed spectral images that are modeled from linear projections. Thus we consider the following models for the observed compressive multispectral and hyperspectral images

$$\begin{array}{rll} \mathbf{Y}_m = & \mathbf{H}_m\mathbf{R}\mathbf{X} + \mathbf{N}_m & = \mathbf{H}_m\mathbf{R}\mathbf{M}\mathbf{A} + \mathbf{N}_m \\ \mathbf{Y}_h = & \mathbf{H}_h\mathbf{X}\mathbf{B}\mathbf{S} + \mathbf{N}_h & = \mathbf{H}_h\mathbf{M}\mathbf{A}\mathbf{B}\mathbf{S} + \mathbf{N}_h \end{array} \tag{1}$$

where $\mathbf{R} \in \mathbb{R}^{n_\lambda \times m_\lambda}$ is the spectral response of the MS sensor (modeling spectral degradations), $\mathbf{B} \in \mathbb{R}^{n\times n}$ is a cyclic convolution operator acting on the bands, $\mathbf{S} \in \mathbb{R}^{n\times m}$ is a spatial operator (satisfying the condition $\mathbf{S}^T\mathbf{S} = \mathbf{I}_m$), $\mathbf{H}_m \in \mathbb{R}^{s\times n_\lambda}$ and $\mathbf{H}_h \in \mathbb{R}^{t\times m_\lambda}$ are the sensing matrices for the HS and MS images, $\mathbf{Y}_m \in \mathbb{R}^{s\times n}$ and $\mathbf{Y}_h \in \mathbb{R}^{t\times m}$ are the observed multi-spectral and hyperspectral compressive images, t and n are the numbers of filters used to sense the HS and MS images and $\mathbf{N}_m, \mathbf{N}_h$ are additive noise terms. Note that a similar fusion model was investigated in [16], except that the observed images were not compressed, i.e., without the presence of the matrices $\mathbf{H}_m$ and $\mathbf{H}_h$. The image restoration problem considered in this paper consists of estimating the high resolution (HR) image $\mathbf{X}$ from the observed measurements $\mathbf{Y}_m$ and $\mathbf{Y}_h$.

B. Problem formulation

Based on the previous models introduced in (1), we propose to consider the following optimization problem in order to estimate the matrices $\mathbf{M}$ and $\mathbf{A}$ from the observed compressive images $\mathbf{Y}_m$ and $\mathbf{Y}_h$

$$\begin{array}{ll} \min\limits_{\mathbf{M},\mathbf{A}} & f(\mathbf{M},\mathbf{A}) + \lambda\varphi(\mathbf{A}) \\ \text{subject to (s.t.)} & \mathbf{A} \geq 0, \quad \mathbf{1}_p^T\mathbf{A} = \mathbf{1}_n^T \\ & 0 \leq \mathbf{M} \leq 1 \end{array} \tag{2}$$

where $f(\mathbf{M},\mathbf{A}) = \frac{1}{2}\|\mathbf{Y}_m - \mathbf{H}_m\mathbf{R}\mathbf{M}\mathbf{A}\|_F^2 + \frac{1}{2}\|\mathbf{Y}_h - \mathbf{H}_h\mathbf{M}\mathbf{A}\mathbf{B}\mathbf{S}\|_F^2$ includes two data fidelity terms related to the MS and HS images, the operator $\varphi(\mathbf{A}) = \|\mathbf{A}\mathbf{D}_h\|_1 + \|\mathbf{A}\mathbf{D}_v\|_1$ is a total variation (TV) regularizer preserving sharp edges or object boundaries [28], λ is a regularization parameter and the products by the matrices $\mathbf{D}_h$ and $\mathbf{D}_v$ correspond to horizontal and vertical discrete differences. Note that $\|\cdot\|_F^2$ computes the Frobenius norm of a matrix and that for any matrix $\mathbf{P} \in \mathbb{R}^{m\times n}$, $\|\mathbf{P}\|_1 = \sum_{j=1}^m \sum_{k=1}^n |P_{j,k}|$ is used for the l_1 norm. Note also that the constraints for $\mathbf{A}$ in (2) are abundance non-negativity and sum-to-one constraints (ANC and ASC constraints) [18] and that the vector $\mathbf{1}_p$ is a $p \times 1$ vector with all ones. Finally, the constraint for the endmember matrix $\mathbf{M}$ expresses the fact that each spectral signature represents the reflectances of different materials that belong to the interval $[0, 1]$.

III. Optimization Method

This section studies a new optimization algorithm for solving (2). Note that this problem is nonconvex with respect to $(\mathbf{A}, \mathbf{M})$ jointly [29], making its resolution challenging. The strategy investigated here is a block coordinate descent (BCD) approach, alternating optimizations with respect to the matrices $\mathbf{A}$ and $\mathbf{M}$ [29]. Note that the optimization problem in (2) is convex with respect to $\mathbf{A}$ (for a fixed $\mathbf{M}$) and with respect to $\mathbf{M}$ (for a fixed $\mathbf{A}$). Thus, it is quite natural to investigate an ADMM algorithm for this problem [30]. The resulting alternating optimization algorithm is detailed in Algorithm 1. Note that the endmember extraction step in Algorithm 1 is just used for the initialization of the endmember matrix. This step first recovers the HS image from $\mathbf{Y}_h$ by using a statistical approach termed compressive projection principal component analysis (CPPCA) [31] and then uses the vertex component analysis (VCA) [24] to extract the endmembers. The optimization steps with respect to $\mathbf{A}$ and $\mathbf{M}$ are detailed in the following sections.

Algorithm 1: Proposed compressive image fusion

Input : $\mathbf{Y}_m$,$\mathbf{Y}_h$,$\mathbf{R}, \mathbf{B}, \mathbf{S}, \mathbf{H}_m, \mathbf{H}_h$
Output: $\hat{\mathbf{A}}$ and $\hat{\mathbf{M}}$
1: $\mathbf{M}^{(0)} = \mathrm{EE}(\mathbf{Y}_h)$ `%Endmember Extraction`
2: **for** $i = 1$ to stopping rule **do**
3: $\mathbf{A}^{(t)} = \min\limits_{\mathbf{A}\in\mathcal{A}} f((\mathbf{M})^{(t-1)}, \mathbf{A}) + \lambda\varphi(\mathbf{A})$ `%See Algorithm 2`
4: $\mathbf{M}^{(t)} = \min\limits_{\mathbf{M}\in\mathcal{M}} f((\mathbf{M}), \mathbf{A}^{(t)})$ `%See Algorithm 3`
5: **end for**

A. Optimization with respect to the abundance matrix $\mathbf{A}$

The minimization problem in (2) with respect to $\mathbf{A}$ (for a fixed $\mathbf{M}$) can be solved by using the ADMM algorithm. Using an auxiliary variable to split the objective function and the constraints, this problem can be rewritten as follows

$$\begin{array}{ll} \min\limits_{\mathbf{A},\mathbf{V}_i} & \|\mathbf{Y}_m - \mathbf{H}_m\mathbf{R}\mathbf{M}\mathbf{V_1}\|_F^2 + \frac{1}{2}\|\mathbf{Y}_h - \mathbf{H}_h\mathbf{M}\mathbf{V_2}\mathbf{S}\|_F^2 \\ & +\lambda\left(\|\mathbf{V_3}\mathbf{D}_h\|_1 + \|\mathbf{V_4}\mathbf{D}_v\|_1\right) + g(\mathbf{V_5}) \\ \text{subject to} & \mathbf{V_1} = \mathbf{A},\ \mathbf{V_2} = \mathbf{A}\mathbf{B},\ \mathbf{V_3} = \mathbf{A}\mathbf{D}_h \\ & \mathbf{V_4} = \mathbf{A}\mathbf{D}_v,\ \mathbf{V_5} = \mathbf{A} \end{array} \tag{3}$$

where $i = 1, ..., 5$. The function $g(\mathbf{V_5})$ is the indicator function on the set $\mathcal{A} = \{\mathbf{A}|\mathbf{A} \geq 0, \mathbf{1}_p^T\mathbf{A} = \mathbf{1}_n^T\}$, i.e., the function g is defined as

$$g(\mathbf{A}) = \begin{cases} 0 & \text{if } \mathbf{A} \in \mathcal{A} \\ \infty & \text{if } \mathbf{A} \notin \mathcal{A}. \end{cases} \tag{4}$$

The augmented Lagrangian associated with (3) is

$$\begin{array}{l} \mathcal{L}(\mathbf{A}, \mathbf{V}_i, \mathbf{G}_i) = \frac{1}{2}\|\mathbf{Y}_m - \mathbf{H}_m\mathbf{R}\mathbf{M}\mathbf{V_1}\|_F^2 \\ +\frac{1}{2}\|\mathbf{Y}_h - \mathbf{H}_h\mathbf{M}\mathbf{V_2}\mathbf{S}\|_F^2 + \lambda\|\mathbf{V_3}\|_1 + \lambda\|\mathbf{V_4}\|_1 + g(\mathbf{V_5}) \\ +\frac{\rho}{2}\|\mathbf{V_1} - \mathbf{A} + \mathbf{G_1}\|_F^2 + \frac{\rho}{2}\|\mathbf{V_2} - \mathbf{A}\mathbf{B} + \mathbf{G_2}\|_F^2 \\ +\frac{\rho}{2}\|\mathbf{V_3} - \mathbf{A}\mathbf{D}_h + \mathbf{G_3}\|_F^2 + \frac{\rho}{2}\|\mathbf{V_4} - \mathbf{A}\mathbf{D}_v + \mathbf{G_4}\|_F^2 \\ +\frac{\rho}{2}\|\mathbf{V_5} - \mathbf{A} + \mathbf{G_5}\|_F^2 \end{array} \tag{5}$$

where $\mathbf{G_1}$,...,$\mathbf{G_5}$ are the scaled dual variables and $\rho \geq 0$ is weighting the augmented Lagrangian term. The exact procedure used for estimating $\mathbf{A}$ is summarized in Algorithm 2 whereas more details are provided below.

Algorithm 2: ADMM algorithm to estimate $\mathbf{A}$

Input : $\mathbf{Y}_m$,$\mathbf{Y}_h$,$\mathbf{R}, \mathbf{B}, \mathbf{S}, \mathbf{H}_m, \mathbf{H}_h, \rho, \mathbf{M}, \geq 0$
Output: $\mathbf{A}^{(k+1)}$
1: $\mathbf{V}^{(0)}, \mathbf{G}^{(0)}$
2: **for** $k = 1$ to stopping rule **do**
3: $\quad \mathbf{A}^{(k+1)} = \min_{\mathbf{A}} \mathcal{L}(\mathbf{A}, \mathbf{V}_i^{(k)}, \mathbf{G}_i^{(k)})$
4: $\quad$ **for** $l = 1$ to 5 **do**
5: $\quad\quad \mathbf{V}_l^{(k+1)} = \min_{\mathbf{V}_l} \mathcal{L}(\mathbf{A}^{(k+1)}, \mathbf{V}_l, \mathbf{V}_i^{(k)}, \mathbf{G}_i^{(k)})$
6: $\quad$ **end for**
7: $\quad \mathbf{G_1}^{(k+1)} = \mathbf{G_1}^{(k)} + \mathbf{V_1}^{(k+1)} - \mathbf{A}^{(k+1)}$
8: $\quad \mathbf{G_2}^{(k+1)} = \mathbf{G_2}^{(k)} + \mathbf{V_2}^{(k+1)} - \mathbf{A}^{(k+1)}\mathbf{B}$
9: $\quad \mathbf{G_3}^{(k+1)} = \mathbf{G_3}^{(k)} + \mathbf{V_3}^{(k+1)} - \mathbf{A}^{(k+1)}\mathbf{D}_h$
10: $\quad \mathbf{G_4}^{(k+1)} = \mathbf{G_4}^{(k)} + \mathbf{V_4}^{(k+1)} - \mathbf{A}^{(k+1)}\mathbf{D}_v$
11: $\quad \mathbf{G_5}^{(k+1)} = \mathbf{G_5}^{(k)} + \mathbf{V_5}^{(k+1)} - \mathbf{A}^{(k+1)}$
12: **end for**

1) Updating $\mathbf{A}$*:* To find the solution to the first minimization problem in (2), we force the derivative of (5) with respect to $\mathbf{A}$ to be zero and solve the resultant system. The solution is $\mathbf{A} = \mathbf{\Xi} \times (\mathbf{2I} + \mathbf{B}\mathbf{B}^T + \mathbf{D}_h\mathbf{D}_h^T + \mathbf{D}_v\mathbf{D}_v^T)^{-1}$, where $\mathbf{\Xi} = (\mathbf{V_1} + \mathbf{G_1}) + (\mathbf{V_2} + \mathbf{G_2})\mathbf{B}^T + (\mathbf{V_3} + \mathbf{G_3})\mathbf{D}_h^T + (\mathbf{V_3} + \mathbf{G_3})\mathbf{D}_v^T + (\mathbf{V_5} + \mathbf{G_5})$. The computation of the matrix $\mathbf{\Xi}$ can be efficiently performed through the use of the FFT due to the circulant matrices in its right-hand side. The complexity of this solution is $\mathcal{O}(p \times n_r \log n_c)$.

2) Updating $\mathbf{V_1}$*:* The minimization problem involving $\mathbf{V_1}$ can be obtained by solving $\partial\mathcal{L}/\partial\mathbf{V_1} = 0$, leading to $\mathbf{V_1} = \mathbf{\Theta}((\mathbf{H}_m\mathbf{R}\mathbf{M})^T\mathbf{H}_m\mathbf{R}\mathbf{M} + \rho\mathbf{I})^{-1}$, where $\mathbf{\Theta} = (\mathbf{H}_m\mathbf{R}\mathbf{M})^T\mathbf{Y}_m + \rho(\mathbf{A} - \mathbf{G_1})$. Note that the inverse term in the expression of $\mathbf{V_1}$ can be pre-computed.

3) Updating $\mathbf{V_2}$*:* To solve the minimization problem involving $\mathbf{V_2}$, we can take advantage of the masking matrix $\mathbf{S}$ to separate $\mathbf{V_2}$ into $\mathbf{V_2S}$ and $\mathbf{V_2}\bar{\mathbf{S}}$, where $\bar{\mathbf{S}}$ is the matrix that selects the pixels not selected by $\mathbf{S}$. This leads to

$$\begin{aligned} \mathbf{V_2S} &= [(\mathbf{H}_h\mathbf{M})^T\mathbf{H}_h\mathbf{M} + \rho\mathbf{I}]^{-1}\mathbf{\Phi} \\ \mathbf{V_2}\bar{\mathbf{S}} &= (\mathbf{AB} - \mathbf{G_2})\bar{\mathbf{S}} \end{aligned} \tag{6}$$

where $\mathbf{\Phi} = (\mathbf{H}_h\mathbf{M})^T\mathbf{Y}_h + \rho(\mathbf{AB} - \mathbf{G_2})\mathbf{S}$.

4) Updating $\mathbf{V_3}$ *and* $\mathbf{V_4}$*:* The minimizations with respect to $\mathbf{V_3}$ and $\mathbf{V_4}$ correspond to pixel-wise vector soft-thresholding operations. More precisely, $\mathbf{V_3} = S_{\lambda/\rho}(\mathbf{A}\mathbf{D}_h - \mathbf{G_3})$ and $\mathbf{V_4} = S_{\lambda/\rho}(\mathbf{A}\mathbf{D}_v - \mathbf{G_4})$, where $S_{\lambda/\rho}$ denotes the pixel-wise soft thresholding operator, with threshold λ/ρ.

5) Updating $\mathbf{V_5}$*:* Minimizing the Lagrangian with respect to $\mathbf{V_5}$ involves the proximal operator of the function g, whose solution is obtained by computing the Euclidean projection of $\mathbf{A} - \mathbf{G_5}$ onto the canonical simplex $\mathcal{A}$, which can be expressed as $\mathbf{V_5} = \Pi_{\mathcal{A}}(\mathbf{A} - \mathbf{G_5})$.

Convergence: In order to guarantee the convergence of Algorithm 2, we need to ensure that the augmented Lagrangian in (5) is a proper convex and closed function, according to the ADMM algorithm. This condition is satisfied since (5) is the sum of nonnegative convex functions [30]. Moreover, since the proper convex optimization function is continuous, it is closed. Thus, the convergence of Algorithm 2 is guaranteed [32].

B. Optimization with respect to the abundance matrix $\mathbf{M}$

Similary, the minimization problem in (2) with respect to $\mathbf{A}$ (for a fixed $\mathbf{M}$) can be solved by using the ADMM algorithm. We split the matrix $\mathbf{M}$ into three auxiliary variables $\mathbf{W}_1$, $\mathbf{W}_2$, $\mathbf{W}_3$ in order to obtain the following problem

$$\begin{aligned} \min_{\mathbf{M},\mathbf{W}_j} \quad & \tfrac{1}{2}\|\mathbf{Y}_m - \mathbf{W_1}\mathbf{A}\|_F^2 + \\ & \tfrac{1}{2}\|\mathbf{Y}_h - \mathbf{W_2}\mathbf{ABS}\|_F^2 + g(\mathbf{W_3}) \\ \text{s.t.} \quad & \mathbf{W_1} = \mathbf{H}_m\mathbf{R}\mathbf{M}, \mathbf{W_2} = \mathbf{H}_h\mathbf{M}, \mathbf{W_3} = \mathbf{M} \end{aligned} \tag{7}$$

where $j = 1, ..., 3$. The function $g(\mathbf{W_3})$ is the indicator function of the set $\mathcal{M} = \{\mathbf{M} | 0 \leq \mathbf{M} \leq 1\}$ defined in (4). The augmented Lagrangian associated with the optimization problem (7) can be written

$$\begin{aligned} &\mathcal{L}(\mathbf{A}, \mathbf{W}_j, \mathbf{G}_j) = \tfrac{1}{2}\|\mathbf{Y}_m - \mathbf{W_1}\mathbf{A}\|_F^2 + \tfrac{1}{2}\|\mathbf{Y}_h - \mathbf{W_2}\mathbf{ABS}\|_F^2 \\ &g(\mathbf{W_3}) + \tfrac{\rho}{2}\|\mathbf{W_1} - \mathbf{H}_m\mathbf{R}\mathbf{M} + \mathbf{G_1}\|_F^2 \\ &+ \tfrac{\rho}{2}\|\mathbf{W_2} - \mathbf{H}_h\mathbf{M} + \mathbf{G_2}\|_F^2 + \tfrac{\rho}{2}\|\mathbf{W_3} - \mathbf{M} + \mathbf{G_3}\|_F^2 \end{aligned} \tag{8}$$

where $\mathbf{G_1}, \mathbf{G_2}, \mathbf{G_3}$ are the scaled dual variables and $\rho \geq 0$ is weighting the augmented Lagrangian term. The ADMM algorithm for $\mathbf{M}$ is summarized in Algorithm 3. More details of its different steps are provided below.

Algorithm 3: ADMM algorithm to estimate $\mathbf{M}$

Input : $\mathbf{Y}_m$,$\mathbf{Y}_h$,$\mathbf{R}, \mathbf{B}, \mathbf{S}, \mathbf{H}_m, \mathbf{H}_h, \mathbf{A}, \rho \geq 0$
Output: $\mathbf{M}^{(k+1)}$
1: $\mathbf{W}^{(0)}, \mathbf{G}^{(0)}$
2: **for** $k = 1$ to stopping rule **do**
3: $\quad \mathbf{M}^{(k+1)} = \min_{\mathbf{M}} \mathcal{L}\left(\mathbf{M}, \mathbf{W}_j^{(k)}, \mathbf{G}_j^{(k)}\right)$
4: $\quad$ **for** $l = 1$ to 3 **do**
5: $\quad\quad \mathbf{W}_l^{(k+1)} = \min_{\mathbf{W}_l} \mathcal{L}\left(\mathbf{M}^{(k+1)}, \mathbf{W}_l, \mathbf{W}_j^{(k)}, \mathbf{G}_j^{(k)}\right)$
6: $\quad$ **end for**
7: $\quad \mathbf{G_1}^{(k+1)} = \mathbf{G_1}^{(k)} + \mathbf{W_1}^{(k+1)} - \mathbf{H}_m\mathbf{R}\mathbf{M}^{(k+1)}$
8: $\quad \mathbf{G_2}^{(k+1)} = \mathbf{G_2}^{(k)} + \mathbf{W_2}^{(k+1)} - \mathbf{H}_h\mathbf{M}^{(k+1)}\mathbf{B}$
9: $\quad \mathbf{G_3}^{(k+1)} = \mathbf{G_3}^{(k)} + \mathbf{W_3}^{(k+1)} - \mathbf{M}^{(k+1)}$
10: **end for**

1) Updating $\mathbf{M}$*:* To update $\mathbf{M}$, we solve the equation $\partial\mathcal{L}/\partial\mathbf{M} = 0$, whose solution is $\mathbf{M} = ((\mathbf{H}_m\mathbf{R})^T\mathbf{H}_m\mathbf{R} + \mathbf{H}_h^T\mathbf{H}_h + \mathbf{I})^{-1}\mathbf{\Sigma}$, where $\mathbf{\Sigma} = (\mathbf{H}_m\mathbf{R})^T(\mathbf{V_1} + \mathbf{G_1}) + \mathbf{H}_h^T(\mathbf{V_2} + \mathbf{G_2}) + \mathbf{V_3} + \mathbf{G_3}$. Note that the inverse term in the right hand side can be pre-computed before the iterations.

2) Updating $\mathbf{W_1}$ *and* $\mathbf{W_2}$*:* The minimization of (8) with respect to $\mathbf{W_1}$ and $\mathbf{W_2}$ has the solutions $\mathbf{W_1} = \mathbf{\Psi_1}(\mathbf{A}\mathbf{A}^T + \rho\mathbf{I})^{-1}$ and $\mathbf{W_2} = \mathbf{\Psi_2}(\mathbf{ABS}(\mathbf{ABS})^T + \rho\mathbf{I})^{-1}$, where $\mathbf{\Psi_1} = \rho(\mathbf{H}_m\mathbf{R}\mathbf{M} - \mathbf{G1}) + \mathbf{Y}_m\mathbf{A}^T$ and $\mathbf{\Psi_2} = \rho(\mathbf{H}_h\mathbf{M} - \mathbf{G2}) + \mathbf{Y}_h(\mathbf{ABS})^T)$. Again, the second term in the right hand can be pre-computed before the iterations.

3) Updating $\mathbf{W_3}$*:* The solution of the minimization problem (7) with respect to $\mathbf{W_3}$ is straightforward to obtain and can be written as $\mathbf{W_3} = \min\left(\max\left(\mathbf{M} - \mathbf{G_3}, 0\right), 1\right)$.

Convergence: The energy function (8) is proper convex as the sum of nonnegative convex functions. Moreover, since the proper convex optimization function is continuous, it is closed. Thus, the convergence of Algorithm 3 is guaranteed [32].

C. Global convergence

Given that the optimization problem in (2) viewed as a function of $\mathbf{A}$ or $\mathbf{M}$ is convex and attains a unique minimum, from Theorem 4.1 in [33], we know that every limit point of the sequence $\{\mathbf{A}^{(t)}, \mathbf{M}^{(t)}\}$ generated by Algorithm 1 is a stationary point of the considered optimization problem.

IV. Simulation Results

This section presents fusion results for HS and MS compressed images using the proposed algorithm based on spectral unmixing. In this experiment, the reference image is the Jasper ridge HS image of size $100 \times 100 \times 198$ [34] [35]. The HS image was generated by applying a spatial blur to the reference image with a 9×9 Gaussian filter with $\sigma = 1.5$ and by downsampling the result by a factor of 2 in each direction. The MS image was generated using a spectral degradation of the reference image resulting in a 4-band MS image. The observed HS and MS images were generated by compressing the HS and MS images with sensing matrices whose entries were generated using a Bernoulli distribution. Indeed, the optical filters can be modeled as realizations of a Bernoulli variable where the value "1" corresponds to a light transmissive element and the value "0" to a blocking element [20], [21]. The compression ratio was 0.5. Additionally, the HS and MS images were both contaminated by additive Gaussian noise, with SNR $= 20$ dB in any spectral band. The number of endmembers present in this scene is $p = 4$.

The fusion results are shown in Fig. 1 whereas quantitative results using different metrics are reported in Table I. Note that the hyperparameters λ and ρ were determined by cross-validation leading to $\lambda = 0.0035$ and $\rho = 0.0065$. The results obtained with the proposed fusion strategy are compared with the FUMI method of [16] which does not use compressive measurements. The estimated endmembers are displayed in Fig. 2 whereas quantitative results related to unmixing are provided in Table II. The quality of the unmixing results is evaluated using the normalized mean square error of the abundance matrix (NMSE_A) and of the endmember matrix (NMSE_M). The spectral distortion of the endmembers is also computed using the metric SAM (SAM_M). These results show that the estimated endmembers are very close to the ground truth. Moreover, Tables I and II show that all indicators used to evaluate the fusion performance are very satisfactory even if the fusion has been performed using images with a significant reduced number of measurements.

TABLE I. Performance of MS + HS fusion methods (Jasper data set): PSNR (dB), UIQI, SAM (degrees), ERGAS, DD ($*10^{-2}$), time (seconds) and the amount of data (%)

Methods	PSNR	UIQI	SAM	ERGAS	DD	Time	Data
Proposed	30.6212	**0.994**	**3.593**	**3.963**	0.917	18.26	**50%**
FUMI	**31.5713**	0.989	3.930	4.757	**1.226**	**3.2783**	100%

TABLE II. Unmixing Performance (Jasper data set): SAM (degrees), NMSE_M (in Decibels), NMSE_A (in Decibels)

Methods	SAM_M	NMSE_M	NMSE_A
Proposed	5.2923	-25.1875	**-27.7375**
FUMI	**3.1393**	**-27.5072**	-2.1902

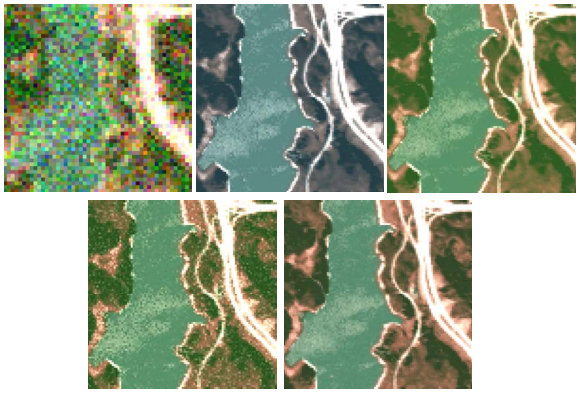

Fig. 1. Fusion results (Jasper Dataset): (Top left) HS image. (Top middle) MS image. (Top right) Reference image. (Bottom left) FUMI method with no compression. (Bottom right) Proposed method with 50% compression.

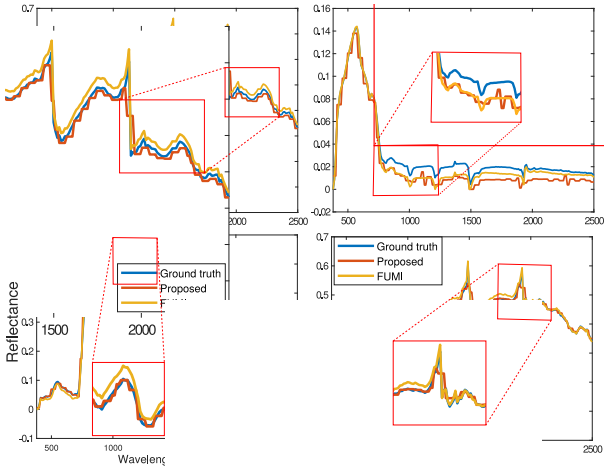

Fig. 2. Four unmixed endmembers for the Jasper dataset obtained using the FUMI and the proposed methods and compared with the ground truth.

V. Conclusions

This paper studied a new algorithm based on spectral unmixing for reconstructing a high-spatial high-spectral image from two compressed MS and HS images. Our results showed that it is possible to recover a high resolution hyperspectral image from compressive spectral imagers, using fewer data samples than conventional techniques. Future work includes the development of a new method for endmember extraction from compressed hyperspectral images to find a better initialization step for endmembers. Regularization parameters were estimated by cross-validation in this work. It would be interesting to study methods allowing these parameters to be estimated directly from the data such as the methods investigated in [36].

REFERENCES

[1] S. May Hsu and H.-h. K. Burke, "Multisensor Fusion with Hyperspectral Imaging Data: Detection and Classification," *Lincoln Laboratory Journal*, vol. 14, no. 1, 2003.

[2] M. E. Schaepman, S. L. Ustin, A. J. Plaza, T. H. Painter, J. Verrelst, and S. Liang, "Earth system science related imaging spectroscopy-An assessment," *Remote Sens. Environ.*, vol. 113, no. 123–137, 2009.

[3] S. V. Panasyuk, S. Yang, D. V. Faller, D. Ngo, R. A. Lew, J. E. Freeman, and A. E. Rogers, "Medical hyperspectral imaging to facilitate residual tumor identification during surgery," *Cancer biology & therapy*, vol. 6, no. 3, pp. 439–446, 2007.

[4] E. K. Hege, D. O'Connell, W. Johnson, S. Basty, and E. L. Dereniak, "Hyperspectral imaging for astronomy and space surviellance," in *Optical Science and Technology, SPIE's 48th Annual Meeting*, 2004, pp. 380–391.

[5] G. A. Shaw and H.-h. K. Burke, "Spectral imaging for remote sensing," *Lincoln Laboratory Journal*, vol. 14, no. 1, pp. 3–28, 2003.

[6] E. M. Middleton, S. G. Ungar, D. J. Mandl, L. Ong, S. W. Frye, P. E. Campbell, D. R. Landis, J. P. Young, and N. H. Pollack, "The earth observing one (eo-1) satellite mission: Over a decade in space," *IEEE J. Sel. Topics Appl. Earth Observ. in Remote Sens.*, vol. 6, no. 2, pp. 243–256, 2013.

[7] D. L. Donoho, "Compressed sensing," *IEEE Trans. inf. Theory*, vol. 52, no. 4, pp. 1289–1306, 2006.

[8] M. Gehm, R. John, D. Brady, R. Willett, and T. Schulz, "Single-shot compressive spectral imaging with a dual-disperser architecture," *Optics Express*, vol. 15, no. 21, pp. 14 013–14 027, 2007.

[9] M. F. Duarte, M. A. Davenport, D. Takbar, J. N. Laska, T. Sun, K. F. Kelly, and R. G. Baraniuk, "Single-pixel imaging via compressive sampling," *IEEE Signal Process. Mag*, vol. 25, no. 2, pp. 83–91, 2008.

[10] C. V. Correa, H. Arguello, and G. R. Arce, "Snapshot colored compressive spectral imager," *JOSA A*, vol. 32, no. 10, pp. 1754–1763, 2015.

[11] G. R. Arce, D. J. Brady, L. Carin, H. Arguello, and D. S. Kittle, "Compressive coded aperture spectral imaging: An introduction," *IEEE Signal Process. Mag.*, vol. 31, no. 1, pp. 105–115, 2014.

[12] H. Arguello and G. Arce, "Spectrally Selective Compressive Imaging by Matrix System Analysis," in *Imaging Appl. Opt. Tech. Pap.* Washington, D.C.: OSA, jun 2012, p. CM4B.5.

[13] L. Loncan, L. B. de Almeida, J. M. Bioucas-Dias, X. Briottet, J. Chanussot, N. Dobigeon, S. Fabre, W. Liao, G. A. Licciardi, M. Simoes *et al.*, "Hyperspectral pansharpening: A review," *IEEE Geosci. Remote Sens. Mag.*, vol. 3, no. 3, pp. 27–46, 2015.

[14] G. Vivone, L. Alparone, J. Chanussot, M. Dalla Mura, A. Garzelli, G. A. Licciardi, R. Restaino, and L. Wald, "A critical comparison among pansharpening algorithms," *IEEE Trans. Geosci. Remote Sens.*, vol. 53, no. 5, pp. 2565–2586, 2015.

[15] B. Zhukov, D. Oertel, F. Lanzl, and G. Reinhackel, "Unmixing-based multisensor multiresolution image fusion," *IEEE Trans. Geosci. Remote Sens.*, vol. 37, no. 3, pp. 1212–1226, 1999.

[16] Q. Wei, J. Bioucas-Dias, N. Dobigeon, J.-Y. Tourneret, M. Chen, and S. Godsill, "Multiband image fusion based on spectral unmixing," *IEEE Trans. Geosci. Remote Sens*, vol. 54, no. 12, pp. 7236–7249, 2016.

[17] N. Yokoya, T. Yairi, and A. Iwasaki, "Coupled nonnegative matrix factorization unmixing for hyperspectral and multispectral data fusion," *IEEE Trans. Geosci. Remote Sens.*, vol. 50, no. 2, pp. 528–537, 2012.

[18] N. Keshava and J. F. Mustard, "Spectral unmixing," *IEEE Signal Process. Mag.*, vol. 19, no. 1, pp. 44–57, 2002.

[19] X. Lin, Y. Liu, J. Wu, and Q. Dai, "Spatial-spectral encoded compressive hyperspectral imaging," *ACM Transactions on Graphics (TOG)*, vol. 33, no. 6, p. 233, 2014.

[20] H. Rueda, H. Arguello, and G. R. Arce, "Dmd-based implementation of patterned optical filter arrays for compressive spectral imaging," *JOSA A*, vol. 32, no. 1, pp. 80–89, 2015.

[21] H. Arguello and G. R. Arce, "Colored coded aperture design by concentration of measure in compressive spectral imaging," *IEEE Trans. Image Process.*, vol. 23, no. 4, pp. 1896–1908, 2014.

[22] H. Arguello and G. R. Arce, "Rank minimization code aperture design for spectrally selective compressive imaging," *IEEE Trans. Image Process.*, vol. 22, no. 3, pp. 941–954, 2013.

[23] I. August, Y. Oiknine, M. AbuLeil, I. Abdulhalim, and A. Stern, "Miniature compressive ultra-spectral imaging system utilizing a single liquid crystal phase retarder," *Scientific reports*, vol. 6, p. 23524, 2016.

[24] J. M. Nascimento and J. M. Dias, "Vertex component analysis: A fast algorithm to unmix hyperspectral data," *IEEE Trans. Geosci. Remote Sens.*, vol. 43, no. 4, pp. 898–910, 2005.

[25] T.-H. Chan, W.-K. Ma, A. Ambikapathi, and C.-Y. Chi, "A simplex volume maximization framework for hyperspectral endmember extraction," *IEEE Trans. Geosci. Remote Sens.*, vol. 49, no. 11, pp. 4177–4193, 2011.

[26] M. E. Winter, "N-findr: An algorithm for fast autonomous spectral endmember determination in hyperspectral data," in *SPIE's International Symposium on Optical Science, Engineering, and Instrumentation*, Denver, CO, USA, 1999, pp. 266–275.

[27] Q. Wei, N. Dobigeon, and J.-Y. Tourneret, "Bayesian fusion of hyperspectral and multispectral images," in *Proc. ICASSP*. Florence, Italy: IEEE, 2014, pp. 3176–3180.

[28] Y. Wang, J. Yang, W. Yin, and Y. Zhang, "A new alternating minimization algorithm for total variation image reconstruction," *SIAM Journal on Imaging Sciences*, vol. 1, no. 3, pp. 248–272, 2008.

[29] D. P. Bertsekas, *Nonlinear programming*. Belmont, MA, USA: Athena scientific, 1999.

[30] S. Boyd, N. Parikh, E. Chu, B. Peleato, and J. Eckstein, "Distributed optimization and statistical learning via the alternating direction method of multipliers," *Foundations and Trends® in Machine Learning*, vol. 3, no. 1, pp. 1–122, 2011.

[31] J. E. Fowler, "Compressive-projection principal component analysis," *IEEE Trans. Image Process.*, vol. 18, no. 10, pp. 2230–2242, 2009.

[32] S. Boyd and L. Vandenberghe, *Convex optimization*. Cambridge, U.K.: Cambridge University Press, 2004.

[33] P. Tseng, "Convergence of a block coordinate descent method for nondifferentiable minimization," *Journal of optimization theory and applications*, vol. 109, no. 3, pp. 475–494, 2001.

[34] F. Zhu, Y. Wang, S. Xiang, B. Fan, and C. Pan, "Structured sparse method for hyperspectral unmixing," *ISPRS Journal of Photogrammetry and Remote Sensing*, vol. 88, pp. 101–118, 2014.

[35] F. Zhu, Y. Wang, B. Fan, G. Meng, S. Xiang, and C. Pan, "Spectral unmixing via data-guided sparsity," *IEEE Trans. Image Process.*, vol. abs/1403.3155, 2014.

[36] M. Pereyra, P. Schniter, E. Chouzenoux, J.-C. Pesquet, J.-Y. Tourneret, A. Hero, and S. McLaughlin, "Tutorial on stochastic simulation and optimization methods in signal processing," *IEEE J. Sel. Topics Signal Process.*, vol. 10, no. 2, pp. 224–241, Mar. 2016.